PCCP

Accepted Manuscript

ROYAL SOCIETY OF CHEMISTRY

www.rsc.org/pccp

2-Octyl Thiophene Based Three Ring Mesogens: Solid State ^{13}C NMR and XRD Investigations

B. Veeraprakash[a], Nitin P. Lobo[b], T. Narasimhaswamy[a]*, and A. B. Mandal[c]

[a]Polymer Lab, [b]Chemical Physics Lab and [c]Chemical Lab,

CSIR-Central Leather Research Institute, Adyar, Chennai 600020, India.

*E-mail:tnswamy99@hotmail.com

Abstract

2-Octyl thiophene based three-ring mesogens namely 4-n-alkoxyphenyl 4-(5-n-octyl-2-thienyl) benzoates are synthesized by employing palladium acetate based direct arylation. The alkoxy terminal is varied with even carbons from C2 to C14 and enantiotropic polymesomorphism is noticed for all the homologs. Accordingly, phase sequence consisting of nematic, smectic A, smectic C and smectic B is seen for mesogens with terminal chains C6, C8, C10 and C12 on cooling the isotropic phase. For mesogens with C2, C4, C8 and C10 terminal alkoxy chains, the mesophase assignment from hot-stage optical microscope and differential scanning calorimeter is further confirmed by variable temperature powder X-ray diffraction measurements. The appearance of smectic B phase is established by noticing sharp and intense peaks both at small-angle as well as wide-angle regions. For a representative mesogen i.e. T10, high-resolution solid-state ^{13}C NMR investigations are carried out in all the viz. nematic, smectic A, smectic C and smectic B phases. The orientational order parameters calculated form ^{13}C-^{1}H dipolar couplings from 2D SAMPI-4 experiments are found to be 0.44, 0.67, 0.73 and 0.79 in nematic, smectic A, smectic C and smectic B mesophases for the center phenyl ring respectively. Remarkably, the thiophene order parameter in all mesophases is found to be higher than phenyl rings and is explained by considering the molecular shape, which has a terminal bend. Further, the mesogens are found to be photoemissive in chloroform solution with an emission band at ~ 410 nm.

1. Introduction

Thiophene is one of the most important structural moieties employed in the construction of molecular materials.[1-3] Thiophene based thermotropic liquid crystals are one such class of materials which generated much interest owing to their opto-electronic and opto-photonic properties.[4-6] The replacement of phenyl ring with thiophene unit in a mesogenic core imparts dramatic change in property characteristics despite their common aromatic character.[7,8] For instance, extensive studies on thiophene based liquid crystals revealed that insertion of thiophene in the mesogenic core increases the optical anisotropy, decreases the melting point, promotes negative dielectric anisotropy and reduces the viscosity.[9-12] Also, thiophene can change the lateral dipole moment of the mesogen and expand the mesophase range too.[12-14] The presence of sulphur atom introduces a significant lateral dipole moment, changes the polarity of the local bonds and the polarizability of the mesogenic core. All these factors substantially influence the molecular self-assembly, transition temperatures, dielectric, optical and other properties of mesogens in comparison with the benzenoid mesogens. Further, it is also observed that the optical properties as well as mesophase characteristics are sensitive to the location of thiophene in the mesogenic core.[13,14] In other words, if the thiophene is located at the terminal position, often nematic phase is observed whereas if it is placed at the centre of the core, smectic mesophases are found. Additionally, the incorporation of 2, 5-disubstituted thiophene in the middle of the core would result in bent structure for the mesogen and often the melting transition is noted to be high due to the C_{2V} symmetry.[15,16] Conversely, if C_{2V} symmetry is broken by introducing two different units at 2, 5-positions, the mesogens are found to show relatively low melting transition with excellent polymesomorphism.[17,18] Among such mesogens, thiophene with phenyl ring core has emerged as interesting liquid crystalline molecules. Thus, the 4-n-alkoxyphenyl 4-(5-n-alkyl-2-thienyl) benzoates serve as important model compounds for understanding the molecular

organization and orientational order since they are polymesomorphic exhibiting good mesophase range. [19, 20]

In recent years, structural studies of thermotropic liquid crystals by the combination of powder X-ray diffraction (XRD) and high resolution solid-state ^{13}C NMR are increasingly becoming popular.[21-24] This is attributed to the ability of these techniques to probe molecular organization by variable temperature X-ray diffraction (VT-XRD) and the molecular dynamics as well as orientational order (solid-state ^{13}C NMR) in different phases. Further, the recent past witnessed the utility of ^{13}C-^{1}H dipolar couplings determined by 2D separated local field (SLF) experiments for finding the orientational constraints and molecular topology of mesogens in their liquid crystalline phases.[25-27] Hence, in this work, we characterize the structures, molecular packing as well as orientational order of 4-n-alkoxyphenyl 4-(5-n-octyl-2-thienyl) benzoates in which thiophene is part of the core unit. Since these mesogens show polymesomorphism with nematic and wide range of smectic phases, the structural characterization of them is attempted by making use of VT-XRD and high-resolution solid-state ^{13}C NMR in liquid crystalline phases.

2. Experimental Section

Materials

2-Octyl thiophene (Alfa Aesar, London), 4-bromobenzoic acid (AVRA, India), 4-benzyloxy phenol, n-bromo alkanes (C8, C10, C12, and C14), ammonium formate and palladium on charcoal (Pd/C, 10%) were purchased from Aldrich, USA and used without further purification. Tetrahydrofuran (THF) and methanol (SD Fine, India) were used as received. Ethyl acetate, diethyl ether, n-hexane, isopropanol, n-heptane, potassium hydroxide, anhydrous sodium sulfate, Celite-540, and silica gel (100–200 mesh) were obtained from Merck, India and used as received. The 4-alkoxy phenols were prepared by our earlier reported procedure.[28]

The synthetic protocols and spectral data of all the intermediates are furnished in ESI while for final mesogens, the spectral data is provided below.

(T2) 4-ethoxyphenyl 4-(5-octylthiophen-2-yl) benzoate: Yield 73%, m.p-117 °C, FT-IR (KBr, cm^{-1}): 3042 (aromatic C-H_{str}), 2960, 2919 (C-H_{str}), 1732 (C=O_{str}), 1605 and 1543 C=C_{str} aromatic), 1466 (C-H_{ben}), 1268, 1192 and 1130 (C-O-C $_{asym\ \&\ sym\ str}$ of ester and ether respectively); ^{1}H NMR (400 MHz, $CDCl_3$): δ 8.16 (d, *J* = 8.0 Hz, 2H), 7.67 (d, *J* = 8.0 Hz, 2H), 7.28 (d, *J* = 3.3 Hz, 1H), 7.12 (d, *J* = 8.6 Hz, 2H), 6.93 (d, *J* = 8.6 Hz, 2H), 6.80 (d, *J* = 3.3 Hz, 1H), 4.03 (m, *J* = 6.9 Hz, 2H), 2.84 (t, *J* = 7.5 Hz, 2H), 1.72 (dd, *J* = 14.4, 7.3 Hz, 2H), 1.42-1.24 (m, 13H), 0.88 (t, *J* = 6.2 Hz, 3H); ^{13}C NMR (101 MHz, $CDCl_3$): δ 165.32, 156.68, 147.88, 144.33, 140.13, 139.60, 130.81, 127.61, 125.51, 125.06, 124.52, 122.45, 115.10, 63.87, 31.88, 31.65, 30.36, 29.35, 29.24, 29.12, 22.69, 14.88 and 14.14.

(T4) 4-butoxyphenyl 4-(5-octylthiophen-2-yl) benzoate: Yield 70%, m.p-100.2 °C, FT-IR (KBr, cm^{-1}): 3012, (aromatic C-H_{str}), 2952, 2921, 2842 (C-H_{str}), 1738 (C=O_{str}), 1605 and 1509 C=C_{str} aromatic), 1401 (C-H_{ben}), 1290, and 1051 (C-O-C $_{asym\ \&\ sym\ str}$ of ester and ether respectively); ^{1}H NMR (400 MHz, $CDCl_3$): δ 8.18 (d, *J* = 8.2 Hz, 2H), 7.69(d, *J* = 8.2 Hz, 2H), 7.30(d, *J* = 4.0 Hz, 1H), 7.14 (d, *J* = 8.0 Hz, 2H), 6.95 (d, *J* = 8.0 Hz, 2H), 6.78 (d, *J* = 4.2 Hz, 1H), 3.95 (t, *J* = 6.4 Hz, 2H), 2.82 (t, *J* = 7.5 Hz, 2H), 1.80-1.65 (m, 4H), 1.54-1.48 (m, 4H), 1.33 (dd, *J* = 32.7, 13.0 Hz, 8H), 0.97 (t, *J* = 7.3 Hz, 6H); ^{13}C NMR (101 MHz, $CDCL_3$): δ 165.28, 156.86, 147.82, 144.23, 140.09, 130.76, 127.58, 125.47, 125.02, 124.48, 122.38, 115.07, 68.08, 31.84, 31.60, 31.30, 30.32, 29.31, 29.20, 29.08, 22.65, 19.22 and 14.10; MS (HRMS): *m/z* calculated for $C_{29}H_{37}O_3S[M+H]^+$ 465.2463, found 465**.**2471.

(T6) 4-(hexyloxy) phenyl 4-(5-octylthiophen-2-yl) benzoate: Yield 72%, m.p-95.8 °C, FT-IR (KBr, cm^{-1}): 3021 (aromatic C-H_{str}), 2953, 2920 (C-H_{str}), 1738 (C=O_{str}), 1605 and 1513 C=C_{str} aromatic), 1472 (C-H_{ben}), 1253, 1102 and 1080 (C-O-C $_{asym\ \&\ sym\ str}$ of ester and ether

respectively); ^{1}H NMR (400 MHz, $CDCl_3$): δ 8.08 (d, J = 8.4 Hz, 2H), 7.59 (d, J = 8.4 Hz, 2H), 7.20 (d, J = 3.6 Hz, 1H), 7.04 (d, J = 8.0 Hz, 2H), 6.85 (d, J = 8.0 Hz, 2H), 6.72 (d, J = 3.5 Hz, 1H), 3.89 (t, J = 6.6 Hz, 2H), 2.76 (t, J = 7.6 Hz, 2H), 1.78-1.59 (m, 4H), 1.48-1.36 (m, 4H), 1.27 (dd, J = 35.6, 22.9, 6.9 Hz, 12H), 0.83 (t, J = 6.9 Hz, 6H); ^{13}C NMR (101 MHz, $CDCl_3$): δ 164.27, 155.87, 146.82, 143.26, 139.11, 138.56, 129.76, 126.61, 124.46, 124.02, 123.48, 121.38, 114.08, 67.42, 30.84, 30.59, 30.57, 29.32, 28.68, 28.30, 28.23, 28.19, 28.08, 24.70, 21.64, 21.59 and 14.08; MS (HRMS): *m/z* calculated for $C_{31}H_{41}O_3S[M+H]^+$ 493.2776, found 493**.**2772.

(T8) 4-(octyloxy) phenyl 4-(5-octylthiophen-2-yl) benzoate: Yield 80%, m.p-95.3 °C, FT-IR (KBr, cm^{-1}): 3104, 3042 (aromatic C-H_{str}), 2954 (C-H_{str}), 1736 (C=O_{str}), 1605, 1513, 1502 (C=C_{str} aromatic), 1464 (C-H_{ben}), 1214, 1081 and 1068 (C-O-C $_{asym\ \&\ sym\ str}$ of ester and ether respectively); ^{1}H NMR (400 MHz, $CDCl_3$): δ 8.19 (d, *J* = 8.6 Hz, 2H), 7.70 (d, *J* = 8.6 Hz, 2H), 7.31 (d, *J* = 3.3 Hz, 1H), 7.15 (d, *J* = 8.2 Hz, 2H), 6.96 (d, *J* = 8.1 Hz, 2H), 6.83 (d, *J* = 3.1 Hz, 1H), 3.99 (t, *J* = 6.5 Hz, 2H), 2.87 (t, *J* = 7.6 Hz, 2H), 1.88-1.73 (m, 4H), 1.53 -1.33 (m, 4H), 1.38 (dd, *J* = 29.5, 9.6 Hz, 16H), 0.93 (t, *J* = 2.7 Hz, 6H); ^{13}C NMR (101 MHz, $CDCl_3$): δ 165.29, 156.91, 147.85, 144.31, 140.15, 139.60, 130.80, 127.66, 125.50, 125.06, 124.51, 122.42, 115.12, 68.46, 31.88, 31.85, 31.64, 30.36, 29.39, 29.35, 29.31, 29.27, 29.24, 29.13, 26.07, 22.69 and 14.13.

(T10) 4-(decyloxy) phenyl 4-(5-octylthiophen-2-yl) benzoate: Yield 70%, m.p-91.8 °C, FT-IR (KBr, cm^{-1}): 3103, 3066 (aromatic C-H_{str}), 2954, 2840 (C-H_{str}), 1737 (C=O_{str}), 1605 (C=C_{str}), 1511, 1468, (C=C_{str}), 1280, 1212 (C-O-C_{str}); ^{1}H NMR (400 MHz, $CDCl_3$): δ 8.16 (d, *J* = 8.1 Hz, 2H), 7.68 (d, *J* = 8.2 Hz, 2H), 7.28 (d, *J* = 3.4 Hz, 1H), 7.13 (d, *J* = 8.7 Hz, 2H), 6.94 (d, *J* = 8.7 Hz, 2H), 6.80 (d, *J* = 4.0 Hz, 1H), 3.96 (t, *J* = 6.5 Hz, 2H), 2.84 (t, *J* = 7.5 Hz, 2H), 1.80 (dd, *J* = 14.4, 7.2 Hz, 2H), 1.71 (dd, *J* = 14.7, 7.2 Hz, 2H), 1.52-1.44 (m, 4H), 1.41-1.25 (m, 20H), 0.89 (t, *J* = 6.3 Hz, 6H); ^{13}C NMR (101 MHz, $CDCl_3$): δ 165.30, 156.90,

147.86, 144.29, 140.15, 139.59, 130.80, 127.65, 125.50, 125.06, 124.51, 122.41, 115.12, 68.46, 31.92, 31.87, 31.63, 30.35, 29.60, 29.58, 29.42, 29.34, 29.30, 29.23, 29.11, 26.06, 22.70, 22.67, 14.13 and 14.12; MS (HRMS): *m/z* calculated for $C_{35}H_{49}O_3S[M+H]^+$ 549.3402, found 549.3393.

(T12) 4-(dodecyloxy) phenyl 4-(5-octylthiophen-2-yl) benzoate: Yield 75%, m.p-95.7 °C, FT-IR (KBr, cm^{-1}): 3019 (aromatic C-H_{str}), 2952, 2934 (C-H_{str}), 1738 (C=O_{str}), 1605 (C=C_{str}), 1541, 1489 (C-H_{ben}), 862, 732; ^{1}H NMR (400 MHz, $CDCl_3$): δ 8.15 (d, *J* = 8.2 Hz, 2H), 7.66 (d, *J* = 8.2 Hz, 2H), 7.28 (d, *J* = 4.0 Hz, 1H), 7.11 (d, *J* = 8.0 Hz, 2H), 6.93 (d, *J* = 8.0 Hz, 2H), 6.79 (d, *J* = 4.0 Hz, 1H), 3.95 (t, *J* = 6.5 Hz, 2H), 2.84 (t, *J* = 7.6 Hz, 2H), 1.85-1.67 (m, 4H), 1.54-1.37 (m, 28H), 0.88 (t, *J* = 6.4 Hz, 6H); ^{13}C NMR (101 MHz, $CDCl_3$): δ 165.34, 156.90, 147.87, 144.27, 140.13, 139.59, 130.81, 127.62, 125.51, 125.06, 124.52, 122.42, 115.10, 68.44, 31.95, 31.89, 31.65, 30.96, 30.36, 29.70, 29.67, 29.64, 29.62, 29.44, 29.39, 29.36, 29.30, 29.25, 29.13, 26.07, 22.73, 22.69, 14.16 and 14.14.

(T14) 4-(tetradecyloxy) phenyl 4-(5-octylthiophen-2-yl) benzoate: Yield 78%, m.p-97.5 °C, FT-IR (cm^{-1}), 3014, 2957, 2918 (C-H_{str}), 1736 (C=O_{str}), 1603 (C=C_{str}), 1525, 1512 (C=C_{str} aromatic), 1279, 1255, 1046 (C-O-$C_{asym\&symstr}$); ^{1}H NMR (400 MHz, $CDCl_3$): δ 8.08 (d, *J* = 8.2 Hz, 2H), 7.60 (d, *J* = 8.2 Hz, 2H), 7.21 (d, *J* = 4.0 Hz, 1H), 7.05 (d, *J* = 8.7 Hz, 2H), 6.86 (d, *J* = 8.7 Hz, 2H), 6.73 (d, *J* = 4.0 Hz, 1H), 3.89 (t, *J* = 6.5 Hz, 2H), 2.77 (t, *J* = 7.6 Hz, 2H), 1.82-1.58 (m, 4H), 1.48 (m, 4H), 1.24 (m, 28H), 0.81 (t, *J* = 6.3 Hz, 6H); ^{13}C NMR (101 MHz, $CDCl_3$): δ 165.32, 156.68, 147.88, 144.33, 140.13, 139.60, 130.81, 127.61, 125.51, 125.06, 124.52, 122.45, 115.10, 63.87, 31.88, 31.65, 30.36, 29.35, 29.24, 29.12, 22.69, 14.88 and 14.14.

Instrumental Details

FT-IR spectra of the compounds were recorded on ABB BOMEM MB3000 spectrometer using a KBr pellet. Both ^{1}H and ^{13}C NMR spectra of the samples were run on a 400 MHz

Bruker Avance-III spectrometer at room temperature using $CDCl_3$ as a solvent and tetramethyl silane (TMS) as an internal reference. The resonance frequencies of ^1H and ^{13}C were 400.23 and 100.64 MHz respectively. LCMS-ESI spectra were recorded on a Bruker Impact-HD spectrometer. Optical polarizing microphotographs were taken using Carl Zeiss Axiocam MRC5 polarizing microscope equipped with Linkam THMS heating stage with TMS 94 temperature programmer. The samples were placed between 12 mm glass cover slips and transferred to heating stage and heated with programmed heating rate. The photomicrographs were taken using Imager A2M digital camera. Differential scanning calorimetry (DSC) traces were recorded using a DSC Q200 instrument with heating rate of 10°C/minute in nitrogen atmosphere. The samples were subjected to two heating and two cooling cycles. The data obtained from second heating and cooling is used for discussion. UV-Visible absorption spectra were recorded on Varian Cary 50 Bio UV-Visible spectrophotometer in chloroform solution and the photoluminescence spectra were measured in chloroform on Varian Cary eclipse fluorescence spectrophotometer.

Variable temperature powder X-ray diffraction (XRD) measurements were carried out on unoriented samples filled in Lindemann capillary of diameter of 1 mm (Hampton Research, Aliso Viejo, CA, USA) using Cu-Kα (λ=1.54 Å) radiation from PANalytical instrument (DY 1042-Empyrean) and a linear detector (PIXcel 3D). The sample temperature was controlled with a precision of 0.1°C using a heater and a temperature controller (Linkam).[29] The gas phase molecular geometries of T8 and T10 mesogens were optimized by using density functional theory (DFT)-based Becke's[30] three parameter hybrid exchange functional and Lee-Yang-Parr correlation functional (B3LYP)[31] method employing 6-31G (d) basis set Gaussian 09W suite of programs.[32] The static solid state ^{13}C NMR experiments were performed at a magnetic field of 9.4 T on Bruker Avance III HD 400 WB NMR spectrometer at resonance frequencies of 400.07 and 100.61 MHz for ^1H and ^{13}C nuclei respectively. A

double resonance 4 mm MAS WVT probe was used to record spectra in the liquid crystalline phases of the sample under static condition. The sample alignment was done by first heating the sample to the isotropic phase and then slowly cooling to the respective mesophases. The 1D ^{13}C NMR spectra in various mesophases were obtained by cross-polarization (CP) scheme with a contact time of 3 ms, number of scans 256, recycle delay of 8 s and 62.5 kHz radio frequency (RF) field strength on both the ^{1}H and ^{13}C channels. High-resolution 2D SLF spectra were acquired by using the SAMPI-4 pulse sequence [33](Fig 1, ESI). Our recent work highlights the usage of this pulse sequence to variety of liquid crystalline systems.[34] The experimental conditions followed for SAMPI-4 were: CP contact time τ = 3 ms, number of t_1 increments 128 and number of scans 28. To minimize RF heating effects, the recycle delay of 16 s was used. The data were zero filled in both the t_2 and t_1 dimensions, yielding a 4096 × 256 real matrix. A shifted sine bell window function was applied to the time domain data and the spectrum was processed in the phase sensitive mode. In all the experiments, ^{1}H 90° pulse length was 4 μs and SPINAL-64[35] decoupling scheme was employed during the carbon signal acquisition with RF field strength of 30 kHz. The variable temperature measurements were carried out using Bruker BVTB-3500 unit and temperature calibration was done by Pb $(NO_3)_2$ sample.[36] The ^{13}C chemical shift was externally referenced to the adamantane methine peak at 29.5 ppm.

3. Results and Discussion

The synthetic route employed for achieving the target mensogens is shown in Scheme 1 (ESI). The acronyms for the final mesogens are given in experimental section and accordingly, T represents the target mesogen while the suffix denotes the length of the terminal alkoxy chain. The core of the mesogen consists of thiophene directly linked to phenyl ring, which is attached to another phenyl ring by ester group. The alkoxy chain with even carbons (C2-C14) serve as terminal unit at one end whereas the octyl chain connected to

thiophene ring act as another terminal unit. The liquid crystalline properties of T6 mesogen is reported earlier by Bunning et al.[37] In the present work, however, for the synthesis of mesogens, palladium based direct arylation is employed for establishing direct link between thiophene and phenyl ring. The direct arylation has become attractive strategy especially for synthesizing thiophene based molecular materials in contrast to traditional cross-coupling reactions as it avoids use of an organometallic reagent that generates a stoichiometric amount of metal waste which is often toxic, difficult to handle, expensive, and require extra synthetic steps.[38-40] The target mesogens as well as the intermediates are well characterized by FT-IR, ^{1}H, and ^{13}C NMR spectroscopy. Fig. 1 shows the planar structure as well as energy-optimized model of T10 mesogen computed from DFT method of quantum chemical calculations.

The FT-IR spectrum of decyloxy mesogen (T10) (Fig. 2, ESI) revealed prominent intense vibrations at 2954, 1737, and 1280 cm^{-1}, which are attributed to C-H asymmetric stretching, ester carbonyl stretching, and C-O-C asymmetric stretching vibrations, respectively. In proton NMR, (Fig. 3, ESI) the expected spectral lines with multiplicities are observed accounting for all the protons of the mesogen. For instance, thiophene ring showed characteristic two doublets (7.28, 6.80 ppm), the two phenyl rings showed four doublets (8.16, 7.68, 7.13, 6.94 ppm) and the terminal OCH_2 of alkoxy chain is distinctly seen as a triplet at 3.96 ppm while the rest of CH_2 protons appeared at 2.84 ppm. These spectral features are in consistent with the molecular structure.

Mesophase assignment by HOPM and DSC

The HOPM examination of T2 (Fig. 4A-C, ESI) reveals the presence of nematic, smectic A (SmA) and crystal E phases. The sample on cooling the isotropic phase exhibits homeotropic domains and birefringent nematic threads[41] that on further cooling coalesce to threaded texture. At 132.6 °C, the sample completely transforms to homeotropy and the corresponding change in DSC (Fig. 5A, ESI) indicates a phase transition to SmA mesophase. On continued

cooling of the sample, at 115.3 °C, the homeotropic region shows dendritic growth and transforms into platelet texture typical of crystal E phase.[42] The crystallization of the sample is noticed on cooling the crystal E phase at 78 °C. The T4 mesogen (Fig. 4D-G, ESI), on cooling the isotropic phase, shows birefringent droplets that coalesce to form threaded texture of nematic phase. The transition from nematic to SmA phase is noticed at 137.1 °C where typical fan texture is noticed.[41] This texture retained till 98.6 °C and on further cooling, the fans become widened indicating change to smectic B (SmB) (ΔH 2.0 k.cal/mole) phase. At 91.4 °C, the sample shows concentric arcs that remains till room temperature and the phase is assigned as crystal E.[43] Since T6, T8 (Fig. 4H-I, ESI), T10 (Fig. 5B, ESI), and T12 homologues show similar phase sequence (Table 1), T10 mesogen is considered for detailed discussion. This sample on cooling the isotropic phase, schlieren texture typical of nematic phase (Fig. 2A) is observed which flashed when subjected to mechanical stress. The presence of SmA phase is confirmed by noticing focal conic fans (Fig. 2B) as well as homeotropic regions on cooling the schilieren nematic phase. Up on further cooling, the focal conic fans of SmA changed to sanded and broken fan texture while the homeotropic regions converted to schilieren texture (Fig. 2C).[44] Thus the phase has been identified as smectic C (SmC) due to these textural features. The sample on continued cooling, further change in texture is noticed at 92.4 °C where the homeotropic region has reappeared (Fig. 2D). Also the sanded and broken region of SmC phase exhibited arc lines for a short duration. However, these lines disappear within a short span and the sanded and broken fan region of the sample transforms to smooth fans (Fig. 2D).[45] These changes suggest that the low temperature mesophase is smectic B (SmB). This phase is retained the characteristic patterns till 62.3 °C before undergoing a change to crystal E phase (Fig. 2E) followed by crystallization. Thus the HOPM examination of T10 mesogen on cooling from the isotropic phase clearly supports the presence of nematic, SmA, SmC and SmB mesophases (Fig. 2A-E). For T14 mesogen, on

cooling the isotropic phase, battonet formation is noticed which coalesces to give focal conic fan texture of SmA phase (Fig. 4J-L, ESI).[41] At 125.0 °C the fan texture changes to sanded and broken fan texture indicating transition from SmA to SmC phase. In DSC, the peak associated with this transition is found to be second order in nature (ΔH=0.02 k.cal/mol) (Fig. 5C, ESI).[46] At 90.5 °C the appearance of arc lines for a short span of time is noticed and on further cooling, smooth fan texture is observed supporting the transition from SmC to SmB phase.[47] In DSC scan, the enthalpy associated with this phase change is 0.77 k.cal/mol. Finally, the crystallization of the sample is noticed at 74.6 °C. The DSC data of all the mesogens support the enantiotropic nature of the mesophases in concurrence with the HOPM findings. The appearance of multiple signals in DSC scans clearly suggests polymesomorphism.[48] The important feature of the DSC data (Table 1) is the second order nature of the SmA to SmC phases and also high enthalpy values for SmC to SmB phase transition.

An examination of the HOPM and DSC data (Table 1) reveals that with increase in terminal chain length, increase in tendency for smectic mesophase across the homologues is apparent. Indeed in T14, the nematic mesophase completely disappears and the sample shows SmA phase directly on cooling the isotropic phase. These features are in consistent with rod-like molecules where by increasing the terminal chain length and keeping the core length constant, the aspect ratio increases which in turn favor lateral interactions that supports smectic phases.[49,50] The remarkable feature of the series is greater tendency for polymesomorphism and the appearance of various smectic mesophases in enantiotropic fashion. The presence of octyl chain in one side of the thiophene not only contributes for reducing the phase transition temperatures but also favor tendency for smectic ordering in view of increase in molecular length. This observation is well supported by the fact that mesogens without octyl chain on thiophene ring i.e 4-alkoxyphenyl 4-(2-thienyl) benzoates

exhibits nematic mesophase alone with relatively low mesophase range.[51] Further in all the homologues, the SmA to SmC transition is found to be second order as indicated by transition enthalpy values from DSC measurements (Table 1).

VT-XRD studies of T8 and T10 mesogens

The existence of polymesomorphism in the synthesized mesogens is further confirmed by VT-XRD. The XRD investigations are carried out for two representative mesogens i.e. T8 (Fig. 3) and T10 (Fig. 6A-C, ESI). The molecular length of these mesogens (L) is arrived using the energy minimized space filled model from DFT method. For T8, the molecular length is found to be 35.7 Å while for T10 the value is 38.2 Å (Fig. 1). The XRD profile of T8 mesogen measured at 138 °C in SmA phase is shown in Fig. 3A. The XRD scan shows sharp and intense reflection at 2θ=2.54º corresponding to layer spacing (d) 34.73 Å. The wide-angle reflection, on the other hand, is a broad hump centered at 2θ=19.48º (Fig. 3A). These features suggest the layer order characteristic of smectic phases.[52,53] By using the length of the mesogen (L) calculated from energy minimized structure, the d/L ratio is found to be 0.97 for T8 at 138 °C. This value is slightly lower than d/L=1 which could be either due to orientational disorder of the molecules within the smectic layers or the terminal chains are not in fully stretched conformation.[53] In SmC, the XRD profile is similar to SmA phase except shift in the 2θ value in the small-angle region. Further, in SmC phase, the d values showed decreasing trend with lowering of temperature.[54] Thus the lowering of d values in SmC phase as against SmA mesophase is due to the tilt of the molecules in the layer. Accordingly, the tilt angle is calculated to be 18-19° from the the d/L ratio in the temperature range 130-100 °C in SmC phase. In SmB phase, XRD pattern show changes both in small-angle and wide-angle region (Fig. 3B). In the small-angle region layer spacing (d) is increased in contrast to SmC phase. Also the wide-angle broad hump noticed both for SmA

and SmC phases is replaced by sharp and intense peak indicating increase in plane positional order.[55] The d/L ratio in Sm B phase is in the range 1.02-1.03 signifying that the molecules are in fully stretched conformation.[56] For T10 mesogen, in addition to 1D XRD, 2D measurements are also carried out both at small angle and wide angle regions (Fig. 7, ESI). The typical images measured at 90 °C (SmB) and 120° C (SmC) are shown in Fig. 7 (ESI) where in the small angle region, sharp ring is noticed for both the mesophases. In the wide angle region, on the other hand, sharp ring is only seen at 90°C whereas diffuse ring is observed at 120°C. Since the mesogen exhibits SmB phase at 90°C, the sharp ring is expected both in the small angle as well as wide angle regions. However, for SmC mesophase (120°C), the sharp ring is only seen in small angle region while the wide angle region exhibites diffuse ring suggesting absence of in plane positional order.

Further, the appearance of crystal E mesophase in HOPM for majority of the mesogens (T2-T8) prompted us to carry out VT-XRD studies. Thus, mesogens T2 and T4 are subjected to XRD investigations with more focus on the wide angle region. In the case of T2 mesogen, in SmA phase at 115°C, the wide angle region shows broad diffuse reflection indicating the liquid like order within the layer. However, in the temperature range 80-100°C, in the wide angle region, an intense reflection at 4.47 Å with additional three low intense peaks at 4.06, 4.00 and 3.22 Å are clearly noticed (Fig. 8A, ESI). These changes upon on cooling the SmA phase suggests the transition to crystal like smectic phase. In literature, [53,57,58] the appearance of three peaks in the wide angle region with typical d values as observed for T2 mesogen in the range 80-100°C is interpreted as signature of crystal E phase. The orthorhombic cell of crystal E phase exhibits similar pattern and hence the phase has been assigned as Crystal E for T2 mesogen. Further the orthogonal nature of the Crystal E

phase is evident from the sharp reflection noticed in the small angle region at q=2.17 nm (28.8Å) which remains same in the temperature range 80-100°C.

For T4 mesogen, the XRD profile at the wide angle region at 105°C shows broad hump indicating the absence of in plane order and liquid like nature of the molecules while at the small angle region sharp and intense reflection is noticed at 2θ = 2.89 (d=30.5 Å) typical of SmA phase. At 95°C, the wide angle XRD profile shows sharp reflection centered at 4.40 Å in contrast to the SmA phase (105°C). However, the small angle peak remained as same (30.5Å) which support the presence of SmB phase. Further, the measurements in the wide angle region in the temperature range 80-90°C shows three reflections at 4.46 Å, 4.11 Å and 3.24 Å similar to T2 mesogen (Fig. 8B, ESI). These additional peaks in contrast to Sm B phase, suggest phase transition to Crystal E with orthorhombic cell arrangement. It is to be noted that in the same temperature range (80-90°C), the small angle sharp reflection remained same (30.5 Å) which additionally support the orthogonal nature of the crystal E phase. Similar features are indeed also observed for T6, T8 and T10 mesogens in the low temperature region indicating the presence of Crystal E phase. The XRD measurements thus substantiate the phase identification carried out by HOPM in the low temperature region for T2-T8 mesogens. Thus the XRD investigation clearly supports the phase assignment carried by HOPM and DSC for the mesogens. Table 2 lists the XRD data for T8 mesogen while for T10 mesogen (Fig. 6A-C, ESI) the data is enlisted in Table 1(ESI).

^{13}C NMR investigation in Liquid crystalline phases

The T10 mesogen which exhibits nematic, SmA, SmC and SmB mesophases on cooling the isotropic phase, is taken as a representative case, for studying the ^{13}C NMR to examine the chemical shift changes as well as order parameter across the mesophase range. Both 1D and 2D experiments were carried in the respective mesophases to get the aligned spectrum from

which ^{13}C chemical shifts as well as ^{13}C-^{1}H dipolar couplings are extracted. To the best of our knowledge, this is the first investigation of finding the molecular order in thiophene based molecular mesogen that exhibits rich polymesomorphism. Since the isotropic chemical shifts are essential for determining the alignment induced chemical shifts, the solution ^{13}C NMR is first examined. The 1D ^{13}C NMR spectrum of T10 mesogen is acquired by cooling the sample from isotropic phase to respective mesophases in magnetic field. For the SLF NMR experiments, SAMPI4 is used to get the 2D spectrum from which ^{13}C chemical shifts as well as ^{13}C-^{1}H dipolar couplings are extracted. The obtained data is used for computing the orientational order parameter in all the phases.

^{13}C NMR of T10 in solution

The proton decoupled ^{13}C NMR of T10 mesogen in $CDCl_3$ recorded at room temperature is shown in Fig. 4A. The mesogen consists of two phenyl rings and ester carbonyl as a linking unit in the core and decyloxy chain at end and octyl chain at 2-position of thiophene act as another terminal. The spectrum shows 13 lines as expected. All these thirteen lines are well resolved in the experimental spectrum and are observed with varying intensities in the region 115-165 ppm. For the terminal decyloxy and octyl chains, the spectrum showed lines in the range 14-68 ppm. To assign the experimental ^{13}C NMR spectrum, ACD Chemsketch (version 3.0) software is used to iterate the spectrum and assigned the chemical shift values of all the core unit carbons of the mesogen (Table 3). The core of the mesogen consists of six methine carbons, two each from phenyl and thiophene rings. The quaternary carbons of the core unit are clearly seen in the range of 127-165 ppm. The spectral lines with high intensities in the interval of 115-130 ppm are attributed to methine carbons of the two-phenyl and thiophene rings. The thiophene methine signals are seen at 124.5 and 125.5 ppm. For the terminal decyloxy and octyl chains, the characteristic oxymethylene and methylene of both carbons are noticed at 68.4 and 31.9 ppm while the two methyl carbons of both the chains are

observed at 14.12 and 14.13 ppm. These spectral features are in conformity with the molecular structure depicted in Fig. 1A.

Static ^{13}C NMR of T10 in various mesophases

The static ^{13}C NMR of T10 in nematic, SmA, SmC and SmB mesophases are carried out by cooling the sample from isotropic phase. For detailed discussion, the static spectrum measured in smectic C phase at 115 °C is considered (Fig. 4C). The spectrum shows well-resolved peaks arising from core unit as well as terminal octyl and decyloxy chains. For the core unit carbons, the chemical shifts are found to be in the range 144.9-223.0 ppm while for the terminal chain carbons, the values are in the span of 12.0-63.0 ppm. A close examination of these chemical shifts and a comparison with solution spectrum indicate the alignment of the molecules in the mesophase. Further, the core unit carbons showed increase in chemical shifts in contrast to solution spectrum whereas the terminal chain carbons exhibited marginal decrease. These changes support that the molecular alignment is parallel to the magnetic field.[59,60] In order to assign the chemical shift values of aligned spectrum, different approaches are adopted. For instance, for the assignment of thiophene methine carbons, the 2D spectrum is used where the separation of thiophene and phenyl ring methine carbons is mainly governed by the magnitude of ^{13}C-^{1}H dipolar couplings. For the ring I the assignments are confirmed by comparing the structurally similar known rod-like mesogens for which the aligned ^{13}C NMR spectrum is available.[61] As a consequence, the ring II assignment become simple and straightforward. In solution ^{13}C NMR, thirteen lines are seen in the range 115-165 ppm arising from core unit carbons including the ester linking unit. In the spectrum recorded in SmC phase, only 12 peaks are noticed for the core unit carbons. The peak appeared at 219.8 ppm arising from non-protonated carbon is relatively more intense in contrast to other quaternary carbons that accounts for two carbons. For the carbons of terminal chains, the solution spectrum shows as many as 17 lines whereas the static spectrum

in smectic C phase shows 8 peaks. This variation is attributed to overlapping of the peaks due to close appearance of chemical shifts owing to the similar chemical environment for many methylene carbons in liquid crystalline phase. However, in 2D spectrum, a better resolution of terminal chain carbons is noticed since the separation of peaks in 2D are mostly governed by ^{13}C-^{1}H dipolar couplings which are direct consequence of orientation with respect to long axis. Table 3 lists the chemical shift assignment of all the core unit carbons. In nematic phase (Fig. 4E), the overlapping of C3 and C8 carbons is noticed while the non-protonated carbons arising from C4 and C9 are resolved. Except these two major changes, the spectral pattern of the other core unit carbons (Fig. 4B-E) appear similar in all the mesophases while clear change in chemical shift values is noticed across the mesophase transition. A plot of chemical shift vs temperature measured in all the mesophases is shown in Fig.9 (ESI) where change in chemical shifts with temperature is unambiguous across the mesophase transitions.

2D SAMPI-4 of T10 in various mesophases

The 2D SAMPI-4 experiments for T10 mesogen are carried out in all the mesophases to get the chemical shifts and ^{13}C-^{1}H dipolar couplings of core unit carbons not only to confirm the chemical shift assignment of 1D data and also to find the molecular order (Fig. 10, ESI). Fig. 5A shows the 2D spectrum of T10 measured in SmC mesophase at 115 °C along with dipolar slices of all core unit carbons (Fig. 5B). In the chemical shift range 140-225 ppm, the spectrum shows 12 contours similar to 1D static spectrum (Fig. 4C) where 12 peaks are seen. The important information available from 2D spectra, however, is the assignment of thiophene ring represented by two methine contours. The phenyl ring methine carbons of the core shows four contours (2.80-3.15 kHz) with a comparable intensity while the thiophene contours are seen with relatively high dipolar couplings (3.5-4.94 kHz). As a result, the thiophene methine carbons appeared as well resolved contours that make their assignment

straightforward. In 1D static spectrum, the assignment of thiophene carbons is not easy since they appear along with phenyl ring methine carbons in the range 140-180 ppm. The ester carbonyl unit of the core is noticed as low intense contour with a ^{13}C-^{1}H dipolar coupling of 0.72 kHz. The very low value is due to the non-protonated nature of the carbon as well as the absence of neighboring protonated carbons. Among the quaternary carbons of core unit i.e. phenyl as well as thiophene rings, the contour appeared at 219.9 ppm is assigned to two carbons owing to high intensity. In 1D spectrum also the peak appeared as more intense indicating the overlapping of C4 and C9. Table 3 lists the ^{13}C-^{1}H dipolar couplings of core unit carbons measured in nematic, SmA, SmC and SmB mesophases.

The local orientational order parameters of phenyl rings as well as thiophene are determined in all the mesophases from the experimental dipolar oscillation frequencies obtained from the SAMPI-4 experiment by following the established protocol. [21-22,25,34,62,63] The dipolar oscillation frequency corresponds directly to the dipolar coupling only for an isolated C–H pair. For a carbon coupled to more than one proton, the dipolar coupling information needs to be extracted from the oscillation frequency. For example, in the case of methine carbons of the phenyl ring, the experimental dipolar frequency has two contributions namely, a coupling to the attached proton $D_{C\text{-}Hi}$ and also a coupling to the remote proton at the ortho position $D_{C\text{-}Ho}$. The measured frequency is given by $[(D_{C\text{-}Hi})^2+(D_{C\text{-}Ho})^2]^{1/2}$. The quaternary carbons have couplings to two equivalent protons at the ortho positions, hence, the dipolar frequency will be $\sqrt{2}*(D_{C\text{-}Ho})$. Further, these dipolar couplings are related to the local order parameters, namely, S_{zz} and $(S_{xx}-S_{yy})$ by the following equation, [63,64]

$$D_{CH} = K\,[½\,(3\cos^2\theta_z - 1)\,S_{zz} + ½\,(\cos^2\theta_x - \cos^2\theta_y)\,(S_{xx} - S_{yy})] \quad (1)$$

where $K=-h\gamma_H\gamma_C/4\pi^2r^3_{CH}$, with γ_H and γ_C are the gyromagnetic ratios of ^{1}H and ^{13}C nuclei respectively, r_{CH} is the inter-nuclear vector, θ_x, θ_y and θ_z are angles between r_{CH} and the

corresponding molecular axes. For the phenyl rings, the molecular frame is defined by taking para-axis (C_2 axis) as the z-axis, the x-axis is in the plane of the ring while the y-axis is perpendicular to the plane. Standard bond distances, r_{CH} = 1.1 Å for the C–H bond and r_{CC}= 1.4 Å for the C–C bond, are considered. To arrive at the best fit, the two C–C–H bond angles are also varied slightly around 120°.[65] By employing the eqn 1, the local order parameters S_{zz} and ($S_{xx} - S_{yy}$) can be calculated from the experimentally determined dipolar frequencies for each of the phenyl rings at different mesophases and are listed in Table 4.

A similar approach is extended to thiophene ring for arriving at the order parameter in different mesophases. For calculating the order parameter of thiophene, the bond angles and bond distances computed from the energy minimized structure of thiophene (DFT) is utilized (Fig. 11, ESI). Accordingly, for thiophene ring the final measured dipolar frequencies for C11 and C12 carbons can be expressed as $[(D_{C11\text{-}H11})^2 + (D_{C11\text{-}H12})^2]^{1/2}$ and $[(D_{C12\text{-}H12})^2+(D_{C12\text{-}H11})^2]^{1/2}$, respectively. For C10 carbon, the dipolar frequency would be $[(D_{C10\text{-}H11})^2+2(D_{C10\text{-}H8})^2]^{1/2}$ while for C13 carbon, the dipolar frequency is given by $[(D_{C13\text{-}H12})^2+2(D_{C13\text{-}H\alpha})^2]^{1/2}$. Since, thiophene is an irregular pentagon, three order parameters namely, S_{zz}, (S_{xx}–S_{yy}) and S_{xz} are required for an arbitrary choice of the axis system.[66] Here, the direction parallel to the C_9-C_{10} bond by which thiophene is directly connected to the phenyl ring-II is chosen as the z-axis, with the anticipation that the order along this direction is likely to be the largest. The fit is initiated with only two order parameter namely, S_{zz} and (S_{xx}–S_{yy}) with an assumption that the other order parameter is likely to be small. The angle β between the z-axis and the C_9-C_{10} bond is also slightly varied in order to improve the quality of the fit. Further the efficiency of the fit is improved by varying the two CCH bond angles ~ ±2 degree. It is observed that the addition of third order parameter namely, S_{xz} did not improve the results significantly. Hence, the S_{zz} and (S_{xx}-S_{yy}) order parameter values listed in Table 5 are considered only for thiophene ring.

A close inspection of Table 4 and 5 reveals certain important trends related to orientational information of different moieties of core units. The order parameters (S_{zz}) of phenyl ring I and ring II are comparable in all the mesophases. With decrease in temperature the S_{zz} values showed increasing trend owing to the higher order of low temperature mesophases. In other words, from nematic mesophase to SmB mesophase, an increase in S_{zz} values is found since the SmB mesophase is more ordered than other mesophases. Further, a slightly higher value of ring II order parameter suggests that the long axis is more close to local axis of ring II. A plot of order parameter versus temperature supports clear changes at the mesophase transition (Fig. 12, ESI). The maximum change is noticed at a transition from nematic to SmA phase. For the case of thiophene ring order parameter also, lowering the temperature resulted in an increase in S_{zz} values similar to phenyl rings. The remarkable feature, however, is higher S_{zz} value for thiophene ring in contrast to phenyl rings in all the phases. To find the reason for this observation, the energy optimized structure of the mesogen is closely scrutinized (Fig. 1B). Since thiophene moiety is substituted at 2 and 5 positions, a bent in the molecular shape at the end of the core is observed from the energy minimized structure. For instance, in arriving at the location of long axis on thiophene ring in fitting the ^{13}C-^{1}H dipolar couplings, initially the para axis of ring II is extended to thiophene ring along the C9-C10 bond. This facilitated in fitting the two thiophene methine dipolar couplings to reach the order parameter (S_{zz}). It is clear from the dipolar couplings of thiophene that the long axis of the mesogen is not in collinear to C11 and C12 carbons that is also evident from energy minimized structure. Thus if the core of the mesogen is visualized from thiophene ring, owing to the di-substitution on thiophene moiety i.e. octyl chain on C13 and phenyl ring II at C10 carbon, a terminal bend is evident from the molecular shape. This in turn is responsible for increase in thiophene order parameter. The experimental evidence for this observation is available from the ratio of order parameters of thiophene (S_{zz} (T)) and ring II

(S_{zz} (II)). By using the relationship S_{zz} (II)/S_{zz} (T) = $P_2(\cos\theta)$,[67] the angle θ between thiophene and phenyl ring is calculated to be 14.3-17.0° in the measured temperature range (Table 5). It is important to note that in a recent investigation of thiophene based bent-core mesogen,[22] where thiophene is linked to phenyl rings via ester at 2,5-positions, the solid state 2D ^{13}C NMR showed high order parameter for the thiophene ring as against the phenyl ring. By comparing the ratios of thiophene and phenyl ring order parameters, a tilt angle of 15.4° is found. This value is in close agreement with the values found in the present investigation between thiophene and phenyl ring II in all the mesophases. Hence it can be concluded that the increase in thiophene order could be due to terminal bent shape of the core owing to the presence of thiophene moiety at one end of the core. Further, a gradual increase in tilt angle of thiophene and phenyl ring II with increase in temperature suggests that in nematic phase the terminal bend is slightly higher.

Optical absorption and emission of mesogens in solution

Fig. 13A (ESI) shows the normalized UV-Vis absorption spectra of all the mesogens in chloroform solution ($2x10^{-6}$ M). The absorption maxima ($^{abs}\lambda_{max}$) is located at ~ 330 nm which is due to π-π* transitions contributed by the core unit of the mesogen. The variation in terminal chain length had little effect on the absorption maxima. Fig. 13B (ESI) shows the normalized fluorescence emission carried out in chloroform solution. The emission spectra were obtained with excitation frequency corresponding to the absorption maxima. It is clear from the spectra that the main emission band is located in the range 400-410 nm. It is noteworthy to mention that the three ring mesogens where thiophene is linked to phenyl ring core through ester carbonyl are found to be non-emissive in chloroform solution.[68] This suggests that, in the present case, where thiophene is connected to phenyl ring directly without a linking unit is responsible for observing emission in visible region. In other words,

the effective π-conjugation between thiophene and the directly linked phenyl ring of the core facilitates the photoemission as noticed in the Fig. 13B (ESI).

4. Conclusion

The structural characterization of 4-n-alkoxyphenyl 4-(5-n-octyl-2-thienyl) benzoates showed that the enantiotropic polymesomorphism is evident even for lower homologs. Further, it was found that the C6-C12 homologs show pentamorphism with nematic, SmA, SmC, SmB and crystal E phases. The evidence for smectic mesophases was clearly noticed from VT-XRD where sharp and intense reflection at small-angle region and a broad hump at wide-angle region are detected except for SmB phase where a sharp reflection is noted both at small - angle as well as wide-angle regions. For all homologs, the SmA to SmC phase change was found to be second order transition as evidenced by DSC. The high resolution solid state 2D ^{13}C NMR of a T10 mesogen in all mesophases viz. nematic, SmA, SmC and SmB phases resulted in ^{13}C-^{1}H dipolar couplings from which the order parameter values are found to be 0.44, 0.67, 0.73 and 0.79 respectively for phenyl ring II. Further, the high order parameter for thiophene moiety in all the mesophases was attributed to terminal bend in the molecular shape. The investigation also revealed that the presence of octyl chain on thiophene moiety of the core substantially contributed not only for lowering the melting transition but also favouring smectic mesophases by enhancing the aspect ratio of the mesogen.

Electronic Supplementary Information (ESI) available: It contains Synthetic details, 2D XRD experimental details, powder XRD data for T10 mesogen, Figure of SAMPI-4 pulse sequence, FT-IR spectrum of T10 mesogen, ^{1}H NMR spectrum of T10 mesogen, HOPM plots, DSC plots, 1D and 2D XRD plots of T10 mesogen, Wide angle XRD profile of T2 and T4 mesogens, plot of ^{13}C chemical shift as a function of temperature, 2D SAMPI-4 spectra of

T10 mesogen, Thiophene model, plot of orientational order parameter as function of temperature, UV-vis plot for T10 mesogen. See DOI: 10.1039/b000000x

Acknowledgments

The authors are thankful to Prof. K. V. Ramanathan, NMR Research Centre, Indian Institute of Science, Bangalore, India for his support and keen interest in this project. Our thanks are also to Dr. V. Subramanian, CLRI, for the quantum chemical calculations. We are grateful to Prof. V. A. Raghunathan and Ms. K. N. Vasudha, Raman Research Institute, Bangalore, India for the powder X-ray measurements. Our thanks are also due to Dr. E. Bhoje Gowd and Dr. S. Nagarajan, CSIR-NIIST, Trivandrum for the WAXS and SAXS experiment of one of the sample. The partial financial support from STRAIT project under XII five year plan of CSIR is duly acknowledged. One of the authors, B. Veeraprakash thanks the Council of Scientific and Industrial Research (CSIR), New Delhi for the financial support in the form of Senior Research Fellowship.

References

1. W. Zhu, *Chem. Soc. Rev*., 2013, **42**, 2039-2058.
2. H. Gallardo, and I. Favarin, *Liq. Cryst*., 1993, **13**, 115-125.
3. A. E. A. Contoret, S. R. Farrar, P. O. Jackson, S. M. Khan, L. May, M. J. O'Neill, E. Nicholls, S. M. Kelly, and G. J. Richards, *Adv. Mater*., 2000, **12**, 971-974.
4. K. Akagi, *In Handbook of Thiophene-based Materials: Applications in Organic Electronics and Photonics*, (Eds., Perepichka, I. F., Perepichka, D.F.) John Wiley & Sons, Chichester, UK, 2009, Chapter **12**, 497.
5. H. Hayasaka, T. Miyashita, M. Nakayama, K. Kuwada, and K. Akagi, *J. Am.Chem. Soc*., 2012, **134**, 3758-3765.
6. A. J. Seed, K. J. Toyne, J. W. Goodby, and M. Hird, *J. Mater. Chem.,* 2000, **10**, 2069-2080.
7. A. J. Seed, *Chem. Soc. Rev*., 2007, **36**, 2046-2069.
8. (a) T. J. Dingemans, and E. T. Samulski, *Liq. Cryst.,* 2000, **27**, 131; (b) T. Narasimhaswamy, D. K. Lee, N. Somanathan, and A. Ramamoorthy, *Chem. Mater*., 2005, **17**, 4567-4569.
9. T. Narasimhaswamy, N. Somanathan, D. K. Lee, and A. Ramamoorthy, *Chem. Mater*., 2005, **17**, 2013-2018.
10. R. Brettle, D. A. Dunmur, C. M. Marson, M. Pinol, and K. Toriyama, *Liq. Cryst*., 1993, **13**, 515-529.
11. A. J Seed, G. Cross, K. J. Toyne, and J. W. Goodby*, Liq. Cryst.*, 2003, **30**, 1089-1107.
12. L. H. Wu, Y. C. Wang, and C.S Hsu, *Liq. Cryst*., 2000, **27**, 1503-1513.
13. M. O'Neill, and S. M. Kelly*, Adv. Mater*., 2011, **23**, 566-584.

14. T. J. Dingemans, N. Sanjeevamurthy, and E. T. Samulski, *J. Phys. Chem. B*., 2001, **105**, 8845-8860.

15. R. Cai, and E. T. Samulski, *Liq. Cryst*., 1991, **9**, 617-634.

16. N. L. Campbell, W. L. Duffy, G. I. Thomas, J. H. Wild, S. M. Kelly, K. Bartle, M. O'Neill, V. Minter and R. P. Tuffin, *J. Mater. Chem*., 2002, **12**, 2706–2721.

17. A. J. Seed, J. T. Kenneth, J. W. Goodby, and D. G. McDonnell, *J. Mater. Chem*., 1995, **5**, 1-11.

18. A. J. Seed, J. T. Kenneth and J. W. Goodby, *J. Mater. Chem***.**, 1995, **5**, 653-661.

19. D. J. Byron, A.S. Matharu, S. N. R. Shirazi, A. R. Tajbakhsh, R. C. Wilson, *Liq. Cryst*., 1993, **14**, 645-652.

20. J. L. Butcher, D. J. Byron, A. S. Matharu, R. C. Wilson, *Liq. Cryst*., 1995, **19**, 387-396.

21. M. Kesava Reddy, K. Subramanyam Reddy, K. Yoga, M. Prakash, T. Narasimhaswamy, A. B. Mandal, N. P. Lobo, K. V. Ramanathan, D. S. Shankar Rao and S. Krishna Prasad, *J. Phys. Chem. B.,* 2013, **117**, 5718-5729.

21.S. Kalaivani, T. Narasimhaswamy, B. B. Das, N. P. Lobo and K. V. Ramanathan, *J. Phys. Chem. B.,* 2011, **115**, 11554-11565.

22. M. Kesava Reddy, E. Varathan, N. P. Lobo, B. B. Das, T. Narasimhaswamy, and K.V. Ramanathan, *J. Phys. Chem. C.*, 2014, **118**, 15044-15053.

24. M. Lehmann, M. Jahr, B. Donnio, R. Graf, S. Gemming, and I. Popov, *Chem. Eur. J*., 2008, **14**, 3562-3576.

25. N. P. Lobo, B. B. Das, T. Narasimhaswamy and K.V. Ramanathan, *RSC Adv*., 2014, **4**, 33383-33390.

26. N. P. Lobo, B. V. N. Phani Kumar, T. Narasimhaswamy, and A. B. Mandal, *Phys.Chem.Chem.Phys*., 2014, **16**, 14713-14721.

27. S. Caldarelli, M. Hong, L. Emsley, and A. Pines *J. Phys. Chem.*, 1996, **100**, 18696-18701.

28. G. Siva Mohan Reddy, T. Narasimhaswamy, and K. Mohana Raju, *New J. Chem.*, 2014, **38**, 4357-4364.

29. S. K. Gupta, S. Setia, S. Sidiq, M. Gupta, S. Kumar and S. K. Pal, *RSC Adv*., 2013, **3**, 12060-12065.

30. A. D. Becke, *J. Chem. Phys*., 1993, **98**, 5648-5652.

31. (a) C.T. Lee, W. T. Yang and R. G. Parr, *Phys. Rev. B*, 1988, **37**, 785-789; (b) R. Ditchfield, *J. Chem. Phys.*, 1972, **56**, 5688-5691; (c) J. R. Cheeseman, G. W. Trucks, T. A. Keith and M. J. Frisch, *J. Chem. Phys.,*1996, **104**, 5497-5509; (d) A. E. Aliev, D. C. Murias and S. Zhou, *J. Mol. Struct.: Theochem*., 2009, **893**, 1-5.

32. M. J. Frisch, G. W. Trucks, H. B. Schlegel, G. E. Scuseria, M. A. Robb, J. R. Cheeseman, G. Scalmani, V. Barone, B. Mennucci and G. A. Petersson et al. GAUSSIAN 09, Revision A.02; Gaussian, Inc.: Wallingford, CT, 2009.

33. A. A. Nevzorov and S. J. Opella, *J. Magn. Reson*., 2007, **185**, 59-70.

34. (a) N. P. Lobo, M. Prakash, T. Narasimhaswamy and K.V. Ramanathan, *J. Phys. Chem. A, 2012*, **116**, 7508-7515. (b) M. Kesava Reddy, K. Subramanyam Reddy, T. Narasimhaswamy, B. B. Das, N. P. Lobo and K. V. Ramanathan, *New J. Chem*., 2013, **37**, 3195-3206; (c) M. Kesava Reddy, E. Varathan, B. Jacintha, N. P. Lobo, A. Roy, T. Narasimhaswamy and K. V. Ramanathan, *Phys. Chem. Chem. Phys.*, 2015, **17**, 5236-5247; (d) B. B. Das, T. G. Ajitkumar and K. V. Ramanathan, *Solid State Nucl. Magn. Reson.*, 2008, **33**, 57-63.

35. B. M. Fung, A. K. Khitrin and K. Ermolaev, *J. Magn. Reson*., 2000, **142**, 97-101.

36. P. A. Beckmann and C. A. Dybowski, *J. Magn. Reson.,* 2000, **146**, 379–380.

37. J. D. Bunning, J. L. Butcher, D. J. Byron, A. S. Mathuru, and R. C. Wilson, *Liq. Cryst*., 1995, **19**, 693-698.

38. D. J. Schipper and K. Fagno*, Chem. Mater.,* 2011, **23**, 1594–1600.

39. L. G. Mercier and M. Leclerc, *Acc. Chem. Res.,* 2013, **46**, 1597-1605

40. I. V. Seregin and V. Gevorgyan, *Chem. Soc. Rev.,* 2007, **36**, 1173–1193.

41. I. Dierking, *Textures of Liquid Crystals,* Wiley-VCH Verlag GmbH, Weinheim, Germany, 2003**.**

42. F. Hentrich, C. Tschierske, S. Diele and C. Sauer, *J. Mater. Chem.,* 1994, **4**, 1547-1558.

43. G. W. Gray and J. W. Goodby, Smectic Liquid Crystals, Heyden, Philadelphia, 1984.

44. J. W. Goodby, G. W. Gray, A. J. Leadbetter and M. A. Mazid, *J. Physique.,* 1980, **41**, 591-595.

45. A. Shanavas, T. Narasimhaswamy and A. S. Nasar, *Aust. J. Chem.*, 2012, **65**, 1426.

46. H.Sackmann*, Pure Appl. Chem*., 1974, **38**, 505-527.48.

47. A. Shanavas, T. Narasimhaswamy, B. V. N. Phani Kumar, and A. S. Nasar, *Can. J. Chem.* 2013, **91**, 196–205.

48. A. Wiegeleben and D. Demus, *Cryst. Res. Technol.,* 1982, **17**, 161-165.

49. G. W. Gray, *Molecular Structure and Properties of Liquid Crystals*, Academic Press: New York, 1962

50. G. R. Luckhurst and G. W. Gray, *The Molecular Physics of Liquid Crystals*, Academic Press: New York, 1979.

51. J. W. Brown, D. J. Byron, D. J. Harwood and R. C. Wilson, *Mol. Cryst. Liq. Cryst*., 1989, **173**,121-140.

52. A. De Vries, *Mol. Cryst. Liq. Cryst*., 1985, **131**, 125-145.

53. (a) J. M. Seddon, *Structural Studies of Liquid Crystals by X-Ray Difraction* in *Hand Book of Liquid Crystals*, *Vol. 1*, ed. D. Demus, J. W. Goodby, G. W. Gray, H. W. Spiess and V. Vill, WILEY-VCH, Weinheim, Germany, 1998, pp 635-679. (b) R. Dabrowski, *Liq. Cryst*., 2015, DOI: 10.1080/02678292.2014.987705.

54. S. Krishna Prasad, D. S. Shankar Rao, S. Sridevi, C. V. Lobo, B. R. Ratna, J. Naciri and R. Shashidhar, *Phys. Rev. Lett*., 2009, **102**, 147802–147805.

55. W. H. De Jau and J. A. De Poorter, *Phys .Lett. A*, 1977, **61**, 114-116.

56. N. Carr, G. W. Gray and S. M. Kelly, *Mol. Cryst. Liq. Cryst*., 1981, **66**, 247-266.

57. S. Diele, S. Tosch, S. Mahnke and D. Demus, *Cryst. Res. Technol.*, 1991, **26**, 809-817.

58. M. Jasiurkowska, A. Budziak, J. Czub, M. Massalska-Arodz and S. Urban, *Liq. Cryst*., 2008, **35**, 513-518.

59. E. E. Burnell and C.A. de Lange, *NMR of Ordered Liquids*, (Eds)., Kluwer Academic Publishers, 2003, The Netherlands.

60. (a) J. W. Emsley, *Nuclear Magnetic Resonance of Liquid Crystals*, (Ed.) Reidel, 1985, Dordrech. (b) R.Y. Dong, D.M. Grant and R.K. Harris, *Encyclopedia of NMR*, (Eds) Wiley, 1996, Chichester. (c) R. Y. Dong, *Prog Nucl. Magn. Reson. Spectrosc*., 2002, **41**, 115. (d) Ramamoorthy, A., Ed. Thermotropic Liquid Crystals: Recent Advances; Springer: Dordrecht, Netherlands, 2007.

61. N. P. Lobo, T. Narasimhaswamy and K. V. Ramanathan, Poster presented at symposium on “New Developments in NMR” and conference of “National Magnetic Resonance

Society (NMRS-2012)" at Indian Institute of Science, Bangalore, India on Feb. 5-8, 2012.

62. (a) C. S. Nagaraja and K. V. Ramanathan, *Liq. Cryst.,* 1999, **26**, 17-21; (b) Z. Gan, *J. Magn. Reson.*, 2000, **143**, 136-143.

63. J. Xu, K. Fodor-Csorba and R. Y. Dong, *J. Phys. Chem. A,* 2005, **109***,* 1998-2005.

64. (a) B. M. Fung, *Prog. Nucl. Magn. Reson. Spectrosc*., 2002, **41**, 171-186. (b) B. M. Fung, *Encycl. Nucl. Magn. Reson.,*1996, **4**, 2744-2751.

65. B. M. Fung, J. Afzal, T. L. Foss and M.-H. Chau, *J. Chem. Phys*., 1986, **85**, 4808-4814.

66. M. Concistr´e, G. De Luca, M. Longeri, G. Pileio and J. W. Emsley, *Chem. Phys. Chem*, 2005, **6**, 1483–1491.

67. (a) R. Y. Dong, *Nuclear Magnetic Resonance Spectroscopy of Liquid Crystals*; World Scientific: Singapore, 2009; (b) V. Domenici, M. Geppi and C. A. Veracini, *Prog. Nucl. Magn. Reson. Spectrosc.,* 2007, **50**, 1-50.

68. (a). M. Kesava Reddy, K. Subramanyam Reddy, M. Prakash, and T.Narasimhaswamy, *Mol. Cryst. Liq. Cryst*., 2013, **582**, 1–14; (b) M. Kesava Reddy, K. Subramanyam Reddy, B. V. N. Phani Kumar and T. Narasimhaswamy, *Mol. Cryst. Liq. Cryst*., 2014, **593**, 1–24.

Table 1: Transition temperatures for the 4-n-alkoxyphenyl 4-(5-n-octyl-2-thienyl) benzoates in second cooling cycle

Code	**Transition temperatures (°C) and enthalpy values in parenthesis (ΔH k.cal/mol)**					
T2	I-N 158.0 (0.203)	N-SmA 130.0 (0.242)	SmA-CrE [111.0] (3.020)	CrE-Cry 74.2 (5.10)	-	-
T4	I-N 150.7 (0.285)	N-SmA 136.5 (0.336)	SmA-SmB [98.6] (2.00)	SmB-CrE 89.6 (0.623)	-	-
T6	I-N 147.3 (0.321)	N-SmA 136.4 (0.315)	SmA-SmC 121.2 (0.0064)	SmC-SmB 94.3 (0.825)	SmB-CrE 73.0 (0.740)	-
T8	I-N 144.9 (0.443)	N-SmA 138.9 (0.245)	SmA-SmC 130.2 (0.0068)	SmC-SmB 94.6 (0.878)	SmB-CrE 68.0 (0.893)	-
T10	I-N 142.6 (0.438)	N-SmA 137.4 (0.217)	SmA-SmC 131.7 (0.0081)	SmC-SmB [92.2] (0.765)	SmB-CrE [63.3] (0.875)	CrE-Cr 58.5 (6.329)
T12	I-N 142.5 (0.37)	N-SmA 137.6 (0.185)	SmA-SmC 133.0 (0.0068)	SmC-SmB [89.6] (0.795)	SmB-Cr 70.5 (11.96)	-
T14	I-SmA 135.0 (1.457)	SmA-SmC 123.6 (0.026)	SmC-SmB [89.5] (0.770)	SmB-Cr 74.6 (14.268)	-	-

[ ] indicates monotropic transition; Cr-Crystal; CrE-Crystal E; SmB-Smectic B; SmC-Smectic C; SmA-Smectic A; N-Nematic; I-Isotropic

Table 2: Variable temperature Powder X-ray diffraction data of T8 mesogen

T(ºC)	d_1 (Å)	d_2 (Å)	d_1/L
138	34.73	4.58	0.97
135	34.73	4.55	0.97
132	34.38	4.50	0.96
130	33.68	4.56	0.94
120	33.68	4.53	0.94
110	33.68	4.55	0.94
100	34.02	4.52	0.95
95	36.61	4.47	1.02
90	36.61	4.44	1.02
85	36.61	4.44	1.02
80	36.61	4.41	1.02
75	36.61	4.41	1.02
65	37.03	4.09	1.03

Table 3: ^{13}C NMR chemical shifts (CS), alignment induced chemical shifts (AIS) and ^{13}C-^{1}H Dipolar Couplings (DC) of T10 mesogen in different liquid crystalline phases.

C. No	Solution (ppm)	90 ˚C			115 ˚C			133 ˚C			138 ˚C		
		CS (ppm)	AIS (ppm)	DC (kHz)	CS (ppm)	AIS (ppm)	DC (kHz)	CS (ppm)	AIS (ppm)	DC (kHz)	CS (ppm)	AIS (ppm)	DC (kHz)
1	156.9	226.5	69.6	1.76	222.9	66.0	1.64	216.2	59.3	1.52	199.8	42.9	1.00
2	115.1	146.2	31.1	3.30	144.9	29.8	3.09	142.5	27.4	2.81	134.7	19.6	1.96
3	122.4	153.3	30.9	3.40	152.1	29.7	3.15	150	27.6	2.88	143.2	20.8	1.86
4	147.9	224.1	76.2	1.78	219.9	72.0	1.65	213.2	65.3	1.50	193.2	45.3	0.98
5	165.3	215.8	50.5	0.89	214	48.7	0.72	209.4	44.1	0.67	196.4	31.1	0.57
6	127.7	207.9	80.2	1.79	204.1	76.4	1.62	198.2	70.5	1.46	178	50.3	0.94
7	130.8	168.7	37.9	3.13	167.1	36.3	2.87	164.2	33.4	2.62	154.9	24.1	1.79
8	125.1	157.3	32.2	3.00	155.3	30.2	2.80	152.3	27.2	2.59	143.2	18.1	1.86
9	139.6	224.1	84.5	1.78	219.9	80.3	1.65	213.2	73.6	1.50	191.9	52.3	0.99
10	140.1	213.6	73.5	1.34	210.2	70.1	1.25	204.9	64.8	1.20	188.2	48.1	0.82
11	124.5	165	40.5	5.34	162.8	38.3	4.94	159.3	34.8	4.38	148.9	24.4	3.15
12	125.5	180.2	54.7	3.90	177.2	51.7	3.57	172.8	47.3	3.25	158.9	33.4	2.36
13	144.3	194.2	49.9	1.30	191.8	47.5	1.19	187.6	43.3	1.14	173.7	29.4	0.70

Table 4: Orientational order parameter for phenyl rings of T10 mesogen in different mesophases[a]

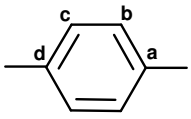

T (°C)	Ring	Angles[b]		S_{zz}	S_{xx}-S_{yy}	Calculated dipolar oscillation frequencies (kHz)			
		θ_b	θ_c			b	c	a	d
90	I	119.9	119.6	0.78	0.072	3.31	3.41	1.78	1.77
	II	120.4	119.9	0.79	0.068	3.13	3.31	1.81	1.79
115	I	119.7	119.6	0.72	0.064	3.10	3.13	1.63	1.63
	II	120.3	120.5	0.73	0.054	2.86	2.80	1.65	1.66
133	I	119.7	119.5	0.66	0.056	2.82	2.88	1.49	1.49
	II	120.1	120.2	0.67	0.04	2.62	2.59	1.49	1.49
138	I	119.3	119.7	0.43	0.042	1.96	1.88	0.98	0.98
	II	119.8	119.5	0.44	0.028	1.79	1.85	0.98	0.97

[a]In the figure above the table, b and c are methine carbons, a and d are quaternary carbons respectively for ring-I and II.

[b] θ_b and θ_c are the angles between para axis (local z-axis) and C_b-H, C_c-H bonds, respectively.

Table 5: Orientational order parameter for thiophene ring at different mesophases[a]

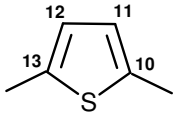

T (°C)	β	Angles[b]		S_{zz}	S_{xx}-S_{yy}	Calculated dipolar oscillation frequencies (kHz)				θ^d
		θ_{11}	θ_{12}			C-11	C-12	C-10[c]	C-13[c]	
90	7	116.0	47.2	0.87	0.056	5.33	3.89	1.40	1.27	14.3
115	7	115.9	47.4	0.81	0.043	4.92	3.58	1.29	1.17	14.9
133	7	116.3	47.6	0.75	0.037	4.40	3.24	1.20	1.09	15.5
138	7	115.6	47.2	0.51	0.025	3.15	2.33	0.80	0.73	17.0

[a]In the figure above the table, 11 and 12 are methine carbons, 10 and 13 are quaternary carbons.

[b] θ_{11} and θ_{12} are the angles between z- axis and C_{11}-H, C_{12}-H bonds, respectively.

[c]For carbons 10 and 13, the contribution from C_8-H (ring-II) and α methylene (alkyl chain) protons, respectively has also been taken into account.

[d]θ is the angle between the local z- axes of thiophene and ring II.

Captions to the Figures

Figure 1: (A) Planar structure and (B) Energy optimized structure of T10 mesogen

Figure 2: HOPM of T10 mesogen on cooling the isotropic phase to (A) Nematic phase at 141.0 ^{o} C, (B) SmA phase at 135.6 ^{o}C (C) SmC at 127.1 ^{o}C, (D) SmB phase at 92.1 ^{o}C, (E) Crystal E phase at 60.1 ^{o}C

Figure 3: High-resolution powder X-ray powder diffraction profile of T8 at (A) 138 ℃ and (B) 75 ℃

Figure 4: ^{13}C NMR spectra of T10 in (A) solution at room temperature, (B) in liquid crystalline phase at 90 ℃ (SmB), (C) 115 ℃ (SmC), (D) 133 ℃ (SmA), and (E) 138 ℃ (Nematic)

Figure 5: (A) 2D SAMPI-4 spectrum of T10 mesogen in smectic C phase at 115 ℃ (B) Dipolar cross sections of corresponding aromatic carbon resonances. Vertical scale for the second column of dipolar cross-sections is raised by a factor of 2.

Figure 1

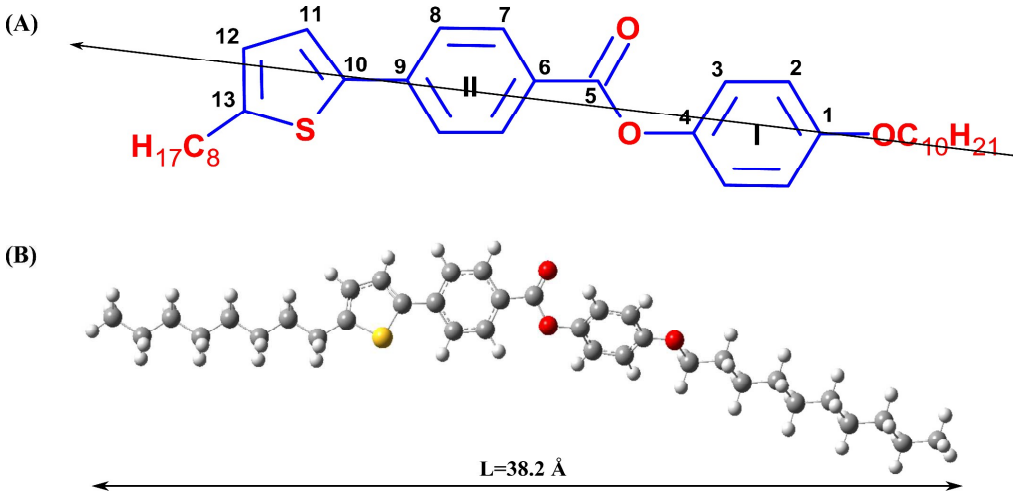

Figure 2

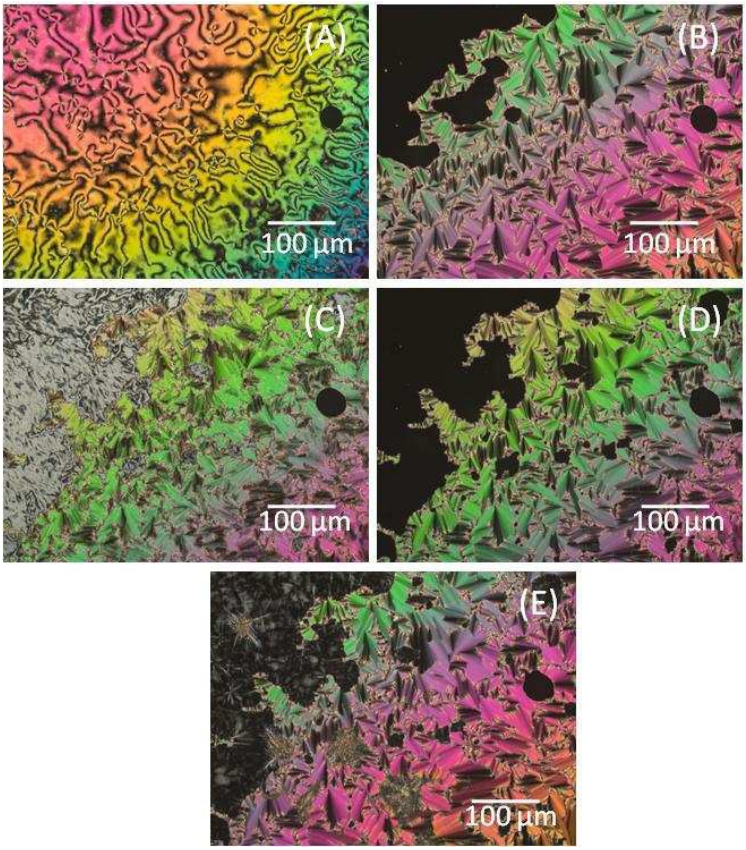

Figure 3

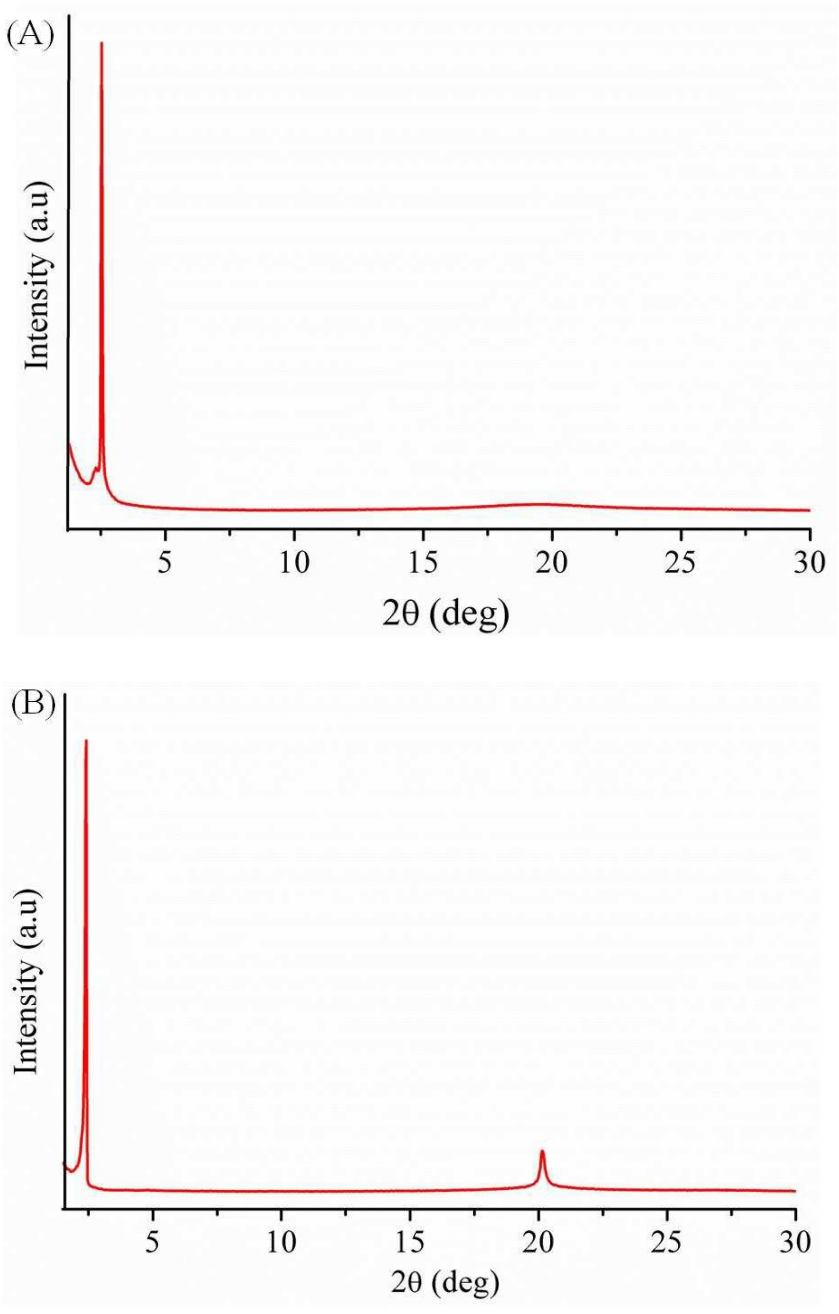

Figure 4

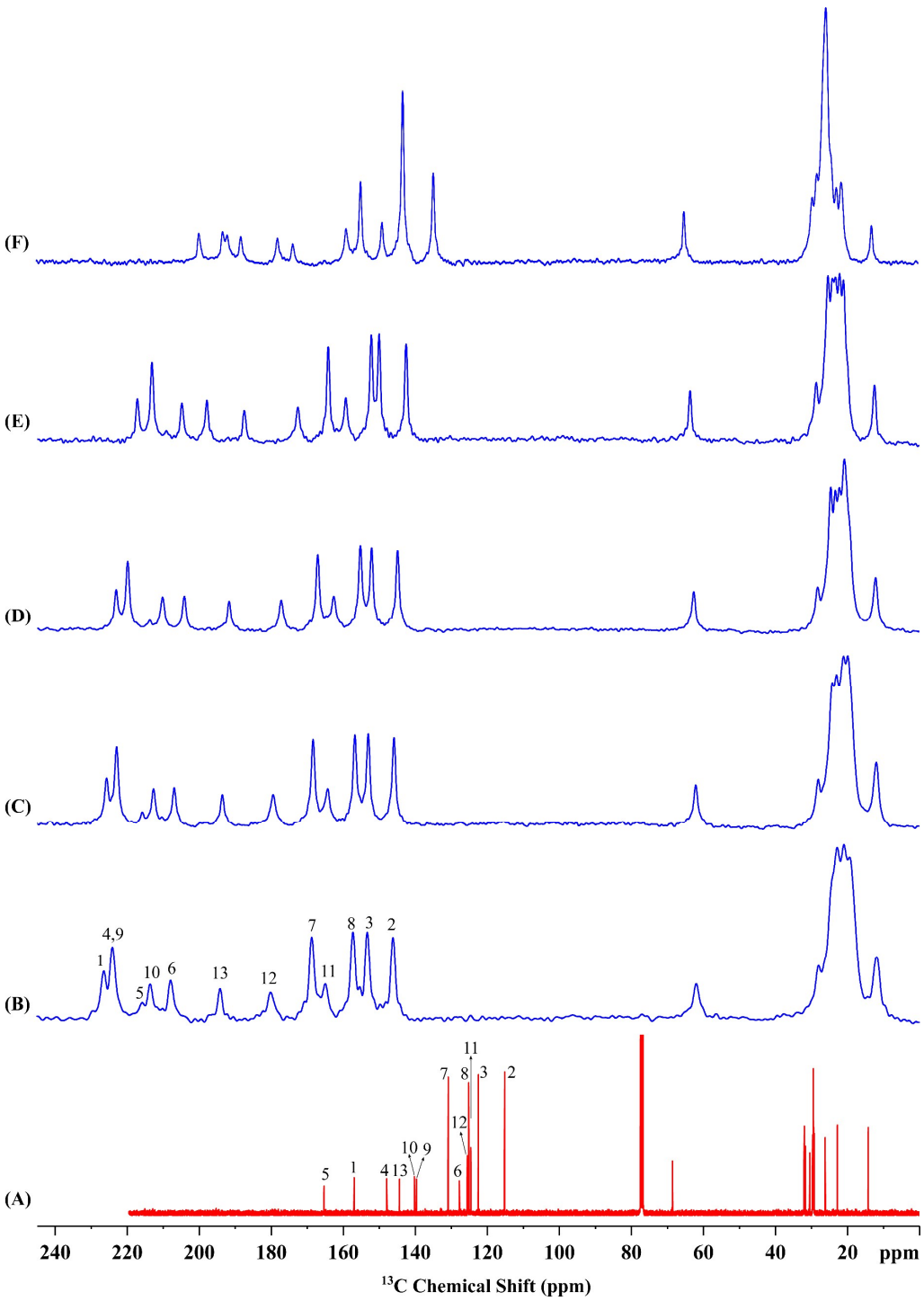

Figure 5